

# Characterizing the dissolution states of a fluorescent probe within a lipid bilayer using molecular dynamics simulations

Ryo Okabe, Natsuomi Ito, Yuya Matsubara, Nozomi Morishita Watanabe, Hiroshi Umakoshi, Kento Kasahara,<sup>a)</sup> and Nobuyuki Matubayasi<sup>b)</sup>

*Division of Chemical Engineering, Graduate School of Engineering Science, Osaka University, Toyonaka, Osaka 560-8531, Japan*

The physicochemical properties of lipid bilayers (membranes) are closely associated with various cellular functions and are often evaluated using absorption and fluorescence spectroscopies. For instance, by employing fluorescent probes that exhibit spectra reflective of the surrounding membrane environment, one can estimate the membrane polarity. Thus, elucidating how such probes are dissolved within the membranes would be beneficial for enabling a deeper interpretation of the spectra. Here, we apply molecular dynamics (MD) simulation with an enhanced sampling method to investigate the dissolution state of 6-propionyl-2-dimethylaminonaphthalene (Prodan) within a membrane composed of 1,2-dioleoyl-*sn*-glycero-3-phosphocholine (DOPC), as well as its variation upon the addition of ethanol as a cosolvent to the aqueous phase. In the absence of ethanol, it is found that the bulky moieties of Prodan (propionyl and dimethylamine groups) prefer to be oriented toward the membrane center owing to the voids existing near the center. The structural change in the membrane induced by the addition of ethanol causes a reduction in the void population near the center, resulting in a diminished orientation preference of Prodan.

## I. INTRODUCTION

Lipids are the major components of cell membranes and form lipid bilayers. The membrane properties are closely associated with cellular functions and modulated by the lipid compositions.<sup>1</sup> For instance, the membrane fluidity of a leukemic cell is enhanced compared to that of the normal cell, and this difference is attributed to the variation in lipid composition due to canceration.<sup>2</sup> Elucidating the membrane properties is crucial also in terms of pharmacokinetics, because drug permeability across the membranes correlates with the membrane polarity and fluidity.<sup>3,4</sup> The membrane permeability varies depending on the cosolvents added to the aqueous phase that faces the membranes, through the structural change in the membrane.<sup>5</sup> It is known that alcohols such as ethanol play a role as permeation enhancers by perturbing the membrane structures.<sup>6,7</sup>

To quantitatively evaluate the membrane properties mentioned above, absorption and fluorescence spectroscopy<sup>8</sup> are commonly employed. In such measurements, fluorescent probes are embedded in the membranes, exhibiting absorption and emission spectra that reflect the local membrane environment. 6-propionyl-2-dimethylaminonaphthalene (Prodan) and 6-dodecanoyl-2-dimethylaminonaphthalene (Laurdan) are widely used probes for analyzing the interfacial and inner regions of the membranes, respectively.<sup>9–11</sup> Owing to their high sensitivity to the surrounding environment,<sup>12–15</sup> these probes exhibit characteristic Stokes shifts that reflect local polarity and hydrogen-bonding interactions within the membrane. The local membrane polarity is often

quantified using the fluorescence intensities at specific wavelengths in the spectrum, expressed as the generalized polarity (GP).<sup>16–19</sup> Very recently, a scheme in systematically analyzing distinct regions within the membrane was constructed based on the fluorescence decays in a series of solvent mixtures.<sup>20,21</sup> In the spectroscopy-based approach, the dissolution states of the probes are represented by their depth within the membrane. Thus, elucidating the dissolution states at the atomistic level would be useful for gaining further physicochemical insights from the spectra.

Molecular dynamics (MD) simulation is a representative computational method to analyze systems of interest in atomistic detail.<sup>22,23</sup> Advances in computational power have made it possible to explore complex systems, including membrane systems.<sup>24,25</sup> Prodan and Laurdan have been extensively investigated using MD simulations as the fluorescent probes embedded in the membranes.<sup>26–29</sup> The quantum mechanics/molecular mechanics (QM/MM) method, combined with molecular dynamics (MD) simulations, is also utilized to analyze the relationship between the dissolution states of probes (structure, position, and orientation) and its spectra.<sup>30–33</sup> In the above studies, the analysis was done for the specific dissolution states. Given that the experimentally observed spectra reflect different dissolution states weighted with the Boltzmann factor, elucidating the probe's dissolution states in terms of thermodynamics would enable a deeper interpretation of the spectra.

In the present study, we elucidate the dissolution state of Prodan based on the free-energy landscape by using the replica-exchange umbrella sampling (REUS) MD simulation.<sup>34–36</sup> The REUS method is an enhanced sampling technique that enables an efficient sampling of the configurations along a predefined coordinate called the reaction coordinate, by employing multiple replicas of the system of interest under different biased potentials.

<sup>a)</sup>Author to whom correspondence should be addressed: kasahara@cheng.es.osaka-u.ac.jp

<sup>b)</sup>Electronic mail: nobuyuki@cheng.es.osaka-u.ac.jp

In the membrane systems, enhanced sampling techniques including the REUS method have been extensively applied to study drug permeation through the membranes for computing the free-energy landscape along a permeation pathway.<sup>37–42</sup> Thus, such methods are expected to provide reliable estimations of the dissolution states of probes.

We apply the REUS method to membrane-probe systems in which Prodan is embedded in membranes composed of 1,2-dioleoyl-*sn*-glycero-3-phosphocholine (DOPC), facing different aqueous phases. As aqueous phases, we examine pure water, 1 M ethanol, and 2 M ethanol solutions. It is well known that the addition of alcohol as a cosolvent induces the structure change in the membranes<sup>7,43–46</sup>, leading to the change in the spectra.<sup>47</sup> Hence, we discuss how the dissolution states are altered upon ethanol addition. Subsequently, the distribution of voids within the membrane and its variation upon ethanol addition are analyzed, as these voids may stabilize specific dissolution states through excluded-volume effects. Since the electrostatic interaction energy between Prodan and its surrounding environment predominantly contributes to its absorption and emission spectra, the interaction energies are also evaluated across different states.

## II. METHODS

In this section, we briefly describe the replica-exchange umbrella sampling (REUS) method.<sup>35</sup> Let us consider a membrane-probe system whose phase-space coordinate is denoted by  $\mathbf{\Gamma}$ , with a potential energy function  $U(\mathbf{\Gamma})$ . In the REUS method, multiple replicas of the system are simulated, each subject to a different biased potential applied along a predefined reaction coordinate  $\zeta$ . The total number of replicas is denoted by  $K$ , and the biased potential applied to the  $i$ th replica is given by  $V_i(\zeta)$ . The functional form of  $V_i(\zeta)$  is defined as

$$V_i(\zeta) = k_i (\zeta - \zeta_i)^2, \quad (1)$$

where  $k_i$  and  $\zeta_i$  represent the force constant and the center of the bias potential, respectively. The modified potential energy of the  $i$ th replica,  $U_i(\mathbf{\Gamma})$ , is expressed as

$$U_i(\mathbf{\Gamma}) = U(\mathbf{\Gamma}) + V_i(\zeta). \quad (2)$$

During the REUS simulation, the configurations are stochastically exchanged between replicas with adjacent indices according to the Metropolis algorithm. This exchange allows the system to escape local minima, thereby accelerating convergence in the free-energy calculation.

The ensemble averages in the unbiased system can be evaluated using the multistate Bennett acceptance ratio (MBAR) method<sup>48</sup>, based on the configurations generated from the REUS simulation, as described below. Let  $\mathbf{\Gamma}_{in}$  ( $n = 1, 2, \dots, N_i$ ) represent the  $n$ th configuration in the  $i$ th replica and  $N_i$  be the number of configurations in

the  $i$ th replica. The free energy of the  $i$ th replica,  $f_i$ , is expressed with

$$f_i = -\frac{1}{\beta} \log \left( \frac{\sum_{j=1}^K \sum_{n=1}^{N_i} \exp[-\beta U_i(\mathbf{\Gamma}_{jn})]}{\sum_{k=1}^K N_k \exp[\beta(f_k - U_k(\mathbf{\Gamma}_{jn}))]} \right), \quad (3)$$

where  $\beta$  is the inverse temperature. Then, the statistical weight of each configuration,  $W(\mathbf{\Gamma}_{in})$ , can be expressed using  $f_i$  as

$$W(\mathbf{\Gamma}_{in}) = \frac{1}{C} \frac{\exp[\beta(U(\mathbf{\Gamma}_{in}))]}{\sum_{k=1}^K N_k \exp[\beta(f_k - U_k(\mathbf{\Gamma}_{in}))]}. \quad (4)$$

Here,  $C$  is the normalization constant that ensures

$$\sum_{i=1}^K \sum_{n=1}^{N_i} W(\mathbf{\Gamma}_{in}) = 1. \quad (5)$$

Using  $W(\mathbf{\Gamma}_{in})$ , one can estimate the ensemble average of arbitrary quantity  $A$ ,  $\langle A \rangle$ , as

$$\langle A \rangle = \sum_{i=1}^K \sum_{n=1}^{N_i} A(\mathbf{\Gamma}_{in}) W(\mathbf{\Gamma}_{in}). \quad (6)$$

## III. COMPUTATIONAL DETAILS

### A. Simulation setups

We investigated the membrane-probe systems composed of 1,2-dioleoyl-*sn*-glycero-3-phosphocholine (DOPC) lipid bilayer and a 6-propionyl-2-dimethylaminonaphthalene (Prodan) (Fig. 1). For the aqueous solutions facing the membrane, pure water, 1 M ethanol, and 2 M ethanol aqueous solutions were used. The force fields for DOPC, Prodan, ethanol, and water were CHARMM36,<sup>49</sup> CHARMM generalized force field (CGenFF),<sup>50</sup> CGenFF, and CHARMM-compatible TIP3P,<sup>51</sup> respectively. The electronic structure of Prodan was calculated using the CAM-B3LYP/cc-pVDZ level calculation.<sup>52,53</sup> Then, the charges from electrostatic potentials using a grid based method (CHelpG) was used for calculating the point charges on the atoms in Prodan.<sup>54</sup> The above quantum chemical calculation was performed using Gaussian 16.<sup>55</sup> The target temperature and pressure were set to 310 K and 1 atm, respectively.

The initial configurations of the membrane were prepared using CHARMM-GUI server.<sup>56–58</sup> The number of DOPC molecules were 128 (64 per leaflet) for all the systems. The numbers of water and ethanol molecules,

( $N_{\text{wat}}$ ,  $N_{\text{etoh}}$ ), were (7680, 0) for pure water, (7250, 140) for 1 M ethanol, and (6910, 280) for 2 M ethanol. The initial configurations of the aqueous phases were built using Packmol.<sup>59</sup>

All the MD simulations were performed with GENESIS 2.0.<sup>60–62</sup> We used the Bussi method for controlling the temperature and pressure.<sup>63</sup> For the initial equilibration stage, we performed MD simulations (1.875 ns in total;  $NVT$  and  $NPT$ ) using the velocity Verlet (VVER) integrator<sup>64</sup> with a time step of 2 fs, applying restraints to the membranes in accordance with the CHARMM-GUI guidelines. Subsequently, the reversible reference system propagator algorithm (r-RESPA) with a time interval of 2.5 fs was used for the simulations under  $NPT$  condition. We conducted the 550 ns MD simulation for further equilibration. After the equilibration, we performed the REUS simulations with 32 replicas. In the REUS simulations, the reaction coordinate was defined as the  $z$ -component of the center of mass (CoM) of Prodan, where the  $z$ -direction is normal to the membrane surface and  $z = 0$  corresponds to the CoM of the membrane. Performing 30 ns MD simulations with automatic tuning of the REUS parameters,<sup>65</sup> the reference positions  $z_i$  (corresponding to  $\zeta_i$  in Eq. (1)) and the force constants  $k_i$  were optimized (Tables S1–S4 of the supplementary material). After the 30 ns simulations without exchange, we conducted 500 ns REUS simulations for production. We also performed two independent 500 ns REUS simulations using the tuned parameters described above for estimating the statistical error. In these runs, 550 ns MD simulation was conducted for equilibration prior to the REUS simulations, starting from different initial configurations. The weights of the configurations in the REUS trajectories were computed by means of the MBAR method implemented in GENESIS.<sup>66</sup> The interaction energy analysis were performed using ERmod 0.3.7.<sup>67</sup>

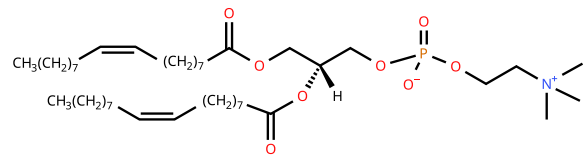
To analyze the void existing inside the membrane, we performed the MD simulations for the membrane systems in the absence of Prodan. The initial configurations were prepared from those of the membrane-probe systems obtained after 550 ns equilibration mentioned above. After deleting the Prodan's coordinates, the energy minimization was conducted. Then, we performed 100 ps  $NVT$  simulations using VVER, followed by 100 ns  $NPT$  simulations using r-RESPA. The last 50 ns were used for analysis.

## IV. RESULTS AND DISCUSSION

### A. Free-energy landscapes

We first examine the two-dimensional free-energy landscape (2D-FEL) as a function of the  $z$ -component of the center of mass (CoM) of Prodan,  $z$ , and the cosine of the tilt angle,  $\cos \theta$  (Fig. 2(a)). The tilt angle,  $\theta$ , is defined as the angle between the membrane normal (the  $z$ -direction)

### (a) DOPC



### (b) Prodan

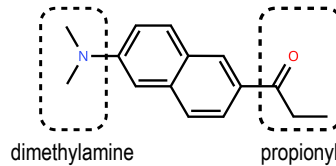


FIG. 1. Chemical structures of (a) 1,2-dioleoyl-*sn*-glycero-3-phosphocholine (DOPC) and (b) 6-propionyl-2-dimethylaminonaphthalene (Prodan).

and the Prodan's molecular axis pointing from the nitrogen atom in the dimethylamine group to the carbonyl carbon atom in the propionyl group. It can be seen from the 2D-FEL for the 0 M ethanol (pure water) case that stable dissolution states appear around  $z \sim 8$  Å, with the molecular axis nearly parallel to the  $z$ -direction ( $\cos \theta \sim \pm 1$ ). On the other hand, the inner region ( $z < 4$  Å) is found to be unfavorable for Prodan especially when its molecular axis is oriented orthogonal to the  $z$ -direction. Then, we define three regions based on  $\cos \theta$  as follows:  $\cos \theta > 0.5$ ,  $\cos \theta < -0.5$ , and  $-0.5 \leq \cos \theta \leq 0.5$  are referred to as vertical (V), vertical' (V'), and horizontal (H), respectively. Since similar profiles are observed in the 2D-FELs for the 1 M and 2 M ethanol cases (Fig. S1 of the supplementary material), this definition is useful for analyzing how the thermodynamic stability of each region changes in the presence of ethanol.

To closely examine the change in thermodynamic stability for each region, we introduce the one-dimensional FELs (1D-FELs) with and without restriction to a specific region X (X = V, V', or H), defined respectively as

$$w_X(z) = -\frac{1}{\beta} \log \frac{\langle \delta(z - z_s(\mathbf{\Gamma})) \Theta_X(\cos \theta) \rangle}{\langle \Theta_X(\cos \theta) \rangle} + C, \quad (7)$$

$$w(z) = -\frac{1}{\beta} \log \langle \delta(z - z_s(\mathbf{\Gamma})) \rangle + C, \quad (8)$$

where  $z_s(\mathbf{\Gamma})$  is the  $z$ -component of CoM of Prodan (solute) for a given phase-space coordinate  $\mathbf{\Gamma}$ , and  $\Theta_X(\cos \theta)$  is the characteristic function that equals unity when  $\cos \theta \in X$  and zero otherwise.  $C$  is the normalization constant, which is determined such that the lowest value of  $w(z)$  is zero. Fig. 2(b)–(d) illustrate the 1D-FELs for the 0, 1, and 2 M ethanol cases, respectively. For all the cases, region V' exhibits the most stable state at  $\sim 8$  Å. It is interesting to note that region V' is more stable than region V, despite the stabilization effect from the electrostatic interaction between Prodan and the aqueous

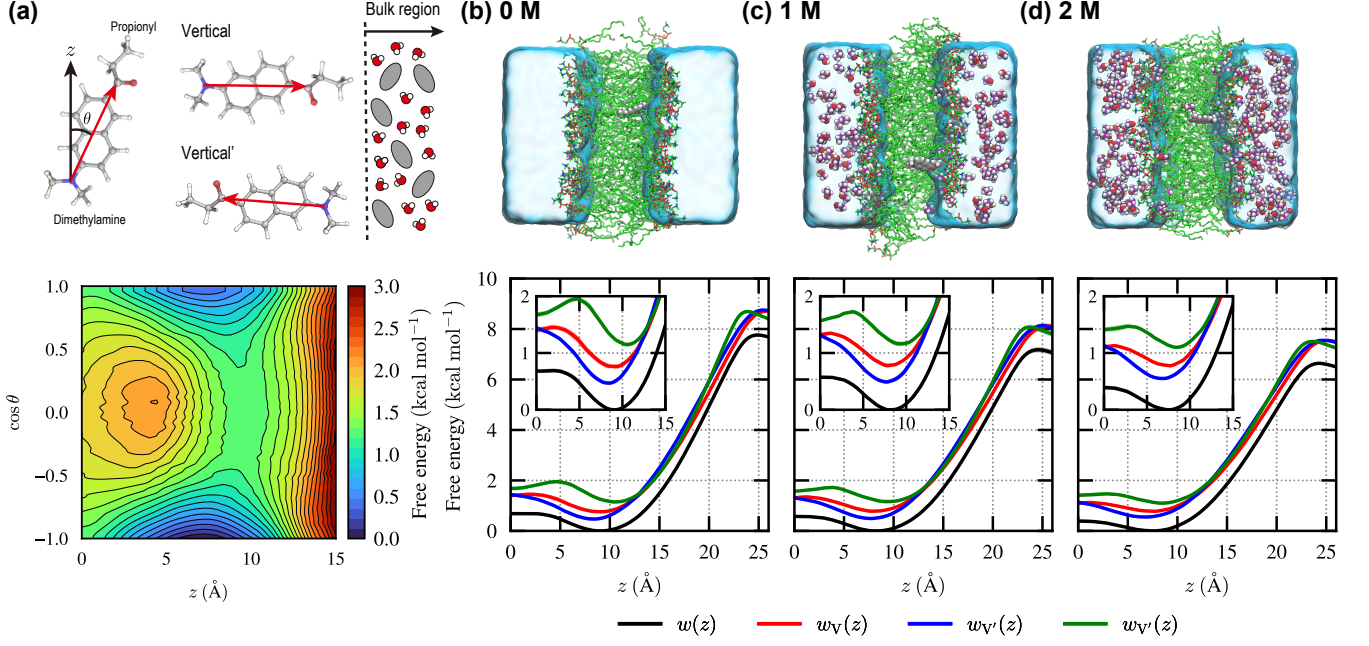


FIG. 2. Free-energy landscapes (FELs) for the dissolution states of Prodan. (a) schematic illustration of Prodan's orientation (top),  $\theta$ , and the 2D-FEL in pure water along the  $z$ -component of CoM for Prodan,  $z$ , and  $\cos \theta$  (bottom), (b)–(d) 1D-FELs along  $z$ ,  $w(z)$  (Eq. (8)), and their decomposition into different regions,  $w_X(z)$  ( $X = V, V'$ , or  $H$ ) (Eq. (7)), for the 0 (pure water), 1 M, and 2 M ethanol cases, respectively.

phase being weaker in region  $V'$  than in region  $V$  due to the increased distance between the propionyl group and the aqueous phase in region  $V'$  (Fig. 2(a)). Region  $H$  at the corresponding  $z$  is found to be unstable compared with regions  $V$  and  $V'$ , as is also seen in the 2D-FEL (Fig. 2(a)). As the ethanol concentration increases, the difference in thermodynamic stability among the different regions at  $z \leq 15$  Å becomes smaller, indicating that the extent of the orientation preference is mitigated by adding ethanol. Regarding the interface ( $z \sim 20 - 25$  Å), a high free-energy barrier is present, reflecting the hydrophobic nature of Prodan, and the difference in the barrier height between different regions is negligibly small. In the presence of ethanol, it is observed that the barrier height is lowered. This trend is consistent with experimental observations that ethanol acts as a permeation enhancer.<sup>6,7</sup>

## B. Decomposition of free energy

In this subsection, we discuss the change in the stability of each state due to the addition of ethanol in terms of the systematic decomposition of free energy according to the classical density functional theory. The free-energy difference between regions  $X_0$  and  $X_1$ ,  $\delta\Delta G^{X_0, X_1}(z)$ ,

given by

$$\delta\Delta G^{X_0, X_1}(z) = -\frac{1}{\beta} \log \frac{\langle \Theta_{X_1}(\cos \theta) \delta(z - z_s(\Gamma)) \rangle}{\langle \Theta_{X_0}(\cos \theta) \delta(z - z_s(\Gamma)) \rangle}, \quad (9)$$

can be decomposed into the difference in the interaction energy of Prodan with the surrounding environment,  $\delta U^{X_0, X_1}(z)$ , and the many-body entropic contribution,  $\delta\Delta G_{MB}^{X_0, X_1}(z)$ , as

$$\delta\Delta G^{X_0, X_1}(z) = \delta U^{X_0, X_1}(z) + \delta\Delta G_{MB}^{X_0, X_1}(z). \quad (10)$$

$\delta\Delta G_{MB}^{X_0, X_1}(z)$  is the difference in the free-energy penalty due to the distortion of the surrounding environment upon the insertion of Prodan between regions  $X_0$  and  $X_1$ .

Fig. 3(a) shows the free-energy difference between regions  $V$  and  $V'$ , denoted as  $\delta\Delta G^{V, V'}(z)$ , together with its decomposition. It is observed that the slightly higher stability of region  $V'$  compared to region  $V$  stems from a more negative value of  $\delta\Delta G_{MB}^{V, V'}$ , suggesting that the extent of membrane distortion upon Prodan insertion is smaller in region  $V'$  than in region  $V$ , especially when Prodan is distant from the membrane center. The positive value of  $\delta U^{V, V'}(z)$  indicates that the stabilization effect of the interaction between Prodan and its surrounding environment is stronger in region  $V$  than in region  $V'$ , although the magnitude of  $\delta U^{V, V'}(z)$  is smaller than that of  $\delta\Delta G_{MB}^{V, V'}(z)$ . As the ethanol concentration increases, the stability of region  $V'$  relative to region  $V$  slightly decreases due to an increase in  $\delta U^{V, V'}(z)$ .



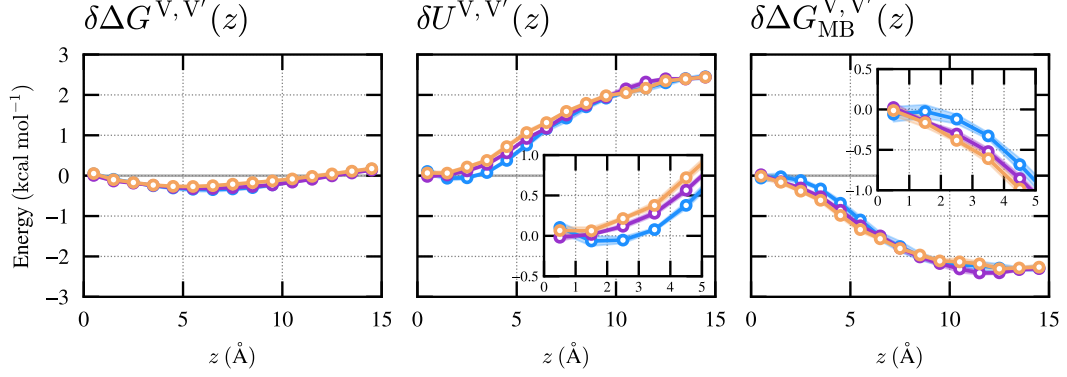
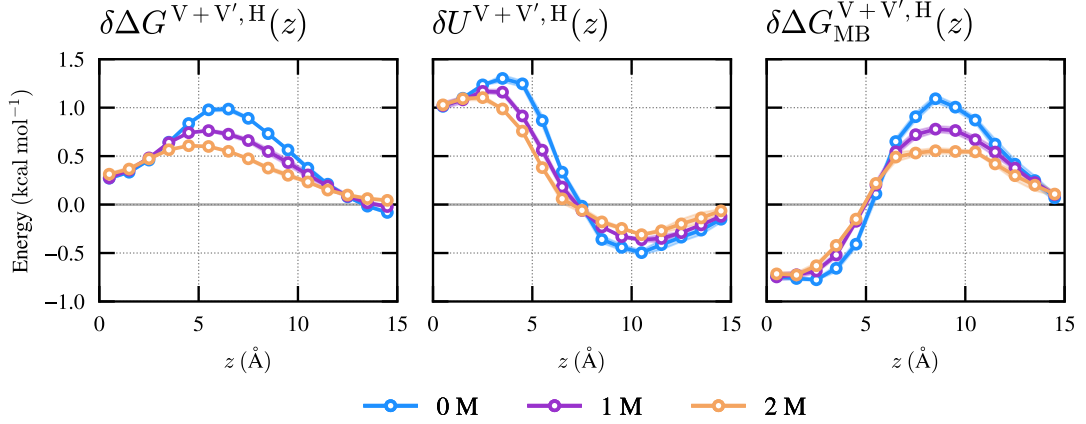
**(a) V vs. V'****(b) V+V' vs. H**

FIG. 3. Differences in the 1D-FELs between different regions,  $\delta\Delta G^{X_0, X_1}$ , and their decomposition into the difference in the interaction energy of Prodan with surrounding environments,  $\delta U^{X_0, X_1}(z)$ , and differences in the many-body entropic contribution,  $\delta\Delta G_{MB}^{X_0, X_1}(z)$ . (a)  $X_0 = V, X_1 = V'$ , (b)  $X_0 = V + V', X_1 = H$ . The left, middle, and right panels of (a) and (b) show the profiles of  $\delta\Delta G^{X_0, X_1}(z)$ ,  $\delta U^{X_0, X_1}(z)$ , and  $\delta\Delta G_{MB}^{X_0, X_1}(z)$ , respectively.

The stability of region H is lower than that of the composite region of V and V', V + V', for the 0 M ethanol case, as indicated by  $\delta\Delta G^{V+V', H}(z)$  (Fig. 3(b)), especially at  $z \sim 6$  Å. Interestingly, the decomposition of  $\Delta G^{V+V', H}(z)$  reveals that the factors contributing to the stabilization or destabilization of region H with respect to region V + V' vary depending on the  $z$ -range. The destabilizing effect of  $\delta U^{V+V', H}(z)$  is evident for  $z \lesssim 7.5$  Å and reaches its maximum around  $z \sim 4$  Å, resulting in the most unstable state in region H at  $z \sim 6$  Å. It is seen that  $\delta\Delta G_{MB}^{V+V', H}(z)$  contributes to the stabilization for  $z \lesssim 5$  Å and its magnitude is smaller than that of  $\delta U^{V+V', H}(z)$ .  $\Delta G_{MB}^{V+V', H}(z)$ , in turn, significantly destabilizes region H around  $z \sim 8$  Å. In the presence of ethanol, region H is found to be stabilized due to the reduction in the destabilizing effects of  $\delta U^{V+V', H}(z)$  and  $\delta\Delta G_{MB}^{V+V', H}(z)$ .

**C. Void-size distribution along  $z$ -direction**

We discuss the structural property of the membrane. According to previous simulation studies on membrane permeation,<sup>68-70</sup> voids, defined as spaces not occupied by atoms, exist within the membrane, particularly near its center. Such voids can reduce the free-energy penalty due to the distortion of the membrane caused by the dissolution of molecules that are related with  $\delta\Delta G_{MB}^{X_0, X_1}$ . Therefore, quantifying these voids is essential for elucidating the dissolution states. In this work, we compute the distribution of the void size ( $\sigma$ ) along the  $z$ -direction,  $P_V(z, \sigma)$ , based on an algorithm developed in the field of computational material science (Appendix A).<sup>71</sup> The trajectory in the absence of Prodan is used for computing  $P_V(z, \sigma)$ .

Fig. 4 shows the  $P_V(z, \sigma)$  for the 0, 1, and 2 M ethanol cases. In all cases, large voids ( $\sigma \geq 3$  Å) are populated near the membrane center. This observation is consistent with the previous studies.<sup>69,70</sup> Such large voids can ac-

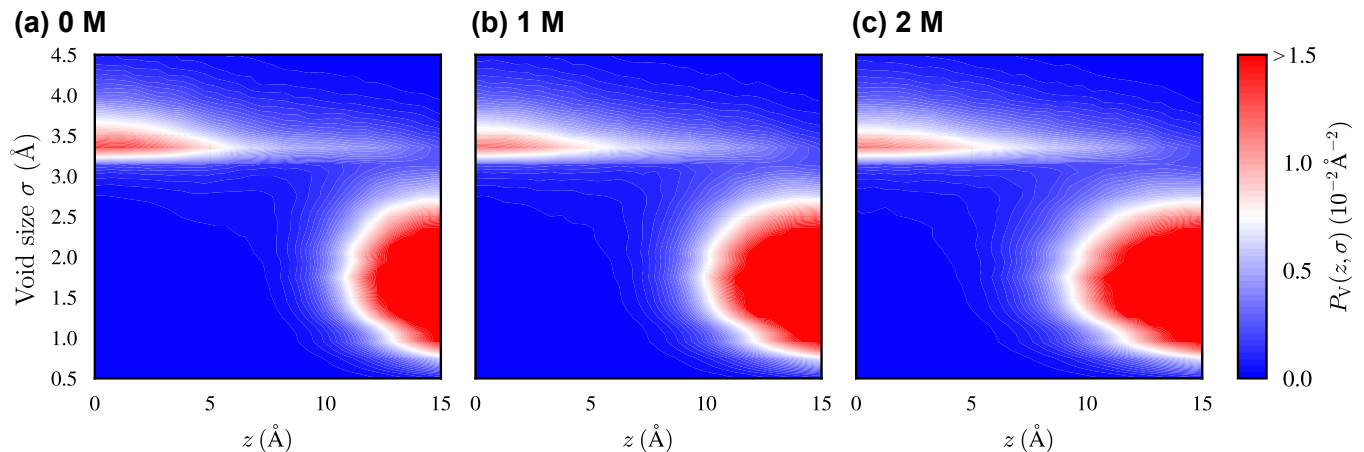


FIG. 4. Void-size distributions along the  $z$ -direction,  $P(z, \sigma)$ , for (a) 0, (b) 1, and (c) 2 M ethanol cases.

commodate bulky molecules or moieties with a low free-energy penalty. Thus, the stabilizing effect of the voids on region H is pronounced for the many-body entropic term when Prodan is located near the membrane center, as all of its atoms are embedded within the membrane center. A broad distribution of  $\sigma$  is observed around  $z = 12 - 15 \text{ \AA}$ , where the glycerol groups of DOPC molecules are located (Fig. S2 of the supplementary material). Since the length of Prodan along its molecular axis is  $\sim 10 \text{ \AA}$ , the presence of voids near the membrane center and  $z = 12 - 15 \text{ \AA}$  is expected to facilitate the preferential dissolution of Prodan in regions V and V', rather than in region H, when Prodan's CoM is located within  $z = 8 - 10 \text{ \AA}$ . In the presence of ethanol, a decrease in the population of large voids near the membrane center is observed, while the overall shape of  $P_V(z, \sigma)$  remains largely changed. This reduction may account for the decreased difference in stability between regions V + V' and H, as reflected by the decrease in  $\Delta G_{\text{MB}}^{\text{V}+\text{V}',\text{H}}$  (Fig. 3(b)).

#### D. Electrostatic interaction of Prodan with surrounding environments

The electrostatic interactions between Prodan and its surrounding environments are elucidated in this subsection. Given that the electrostatic interactions dominantly contribute to the excitation properties, analyzing the interaction patterns is beneficial for discussing the connection between the dissolution state and the excitation behavior.

In Fig. 5, the distributions of the electrostatic interaction for different dissolution states, V, V', and H, are illustrated. The distributions are calculated from snapshots in which the CoM of Prodan is located closer to the membrane center than the average position of the phosphorus atoms in the DOPC molecules. For region V (Fig. 5(a)), there are two peaks at  $\sim -7 \text{ kcal mol}^{-1}$  and  $\sim -1 \text{ kcal mol}^{-1}$ , and the shape of the distribution is

hardly changed upon the addition of ethanol. As revealed by the decomposition into contributions from DOPC and solvent (water and ethanol), the peak at  $\sim -7 \text{ kcal mol}^{-1}$  originates from the solvent. Since the propionyl moiety is oriented toward the membrane-solvent interface in region V and can strongly interact with the solvent, it is reasonable that the solvent contributes to this peak. It can be seen that the peak at  $\sim -1 \text{ kcal mol}^{-1}$  stems from both the DOPC and solvent. Regarding region V' (Fig. 5(b)), only a broad distribution centered at  $\sim -2 \text{ kcal mol}^{-1}$  is observed. Since the dimethylamine group is located near the membrane-solvent surface in region V', the absence of the peak observed at the more negative value in region V reflects the lower hydrophilicity of the dimethylamine group compared with the propionyl group. As the ethanol concentration increases, the peak of the interaction with DOPC and solvent shifts in a positive direction. This shift is caused by the slight weakening of the interaction with DOPC. As shown in Fig. 5(c), region H exhibits a distribution in which the interaction with DOPC and solvent is more negative than  $-6 \text{ kcal mol}^{-1}$ , similar to region V. Adding ethanol increases the population around  $\sim -1 \text{ kcal mol}^{-1}$ , and this change clearly originates from DOPC and leads to a weakened interaction of Prodan with DOPC.

#### V. CONCLUSIONS

In this study, we investigated the dissolution of Prodan within a lipid bilayer composed of 1,2-dioleoyl-*sn*-glycero-3-phosphocholine (DOPC) using the molecular dynamics (MD) simulation with the replica-exchange umbrella sampling (REUS) method. Employing the REUS method enables the evaluation of free-energy landscapes (FELs) for the dissolution state with high statistical reliability. The response of the dissolution states to the addition of ethanol as a cosolvent in the aqueous phase was also examined, given that ethanol is known to

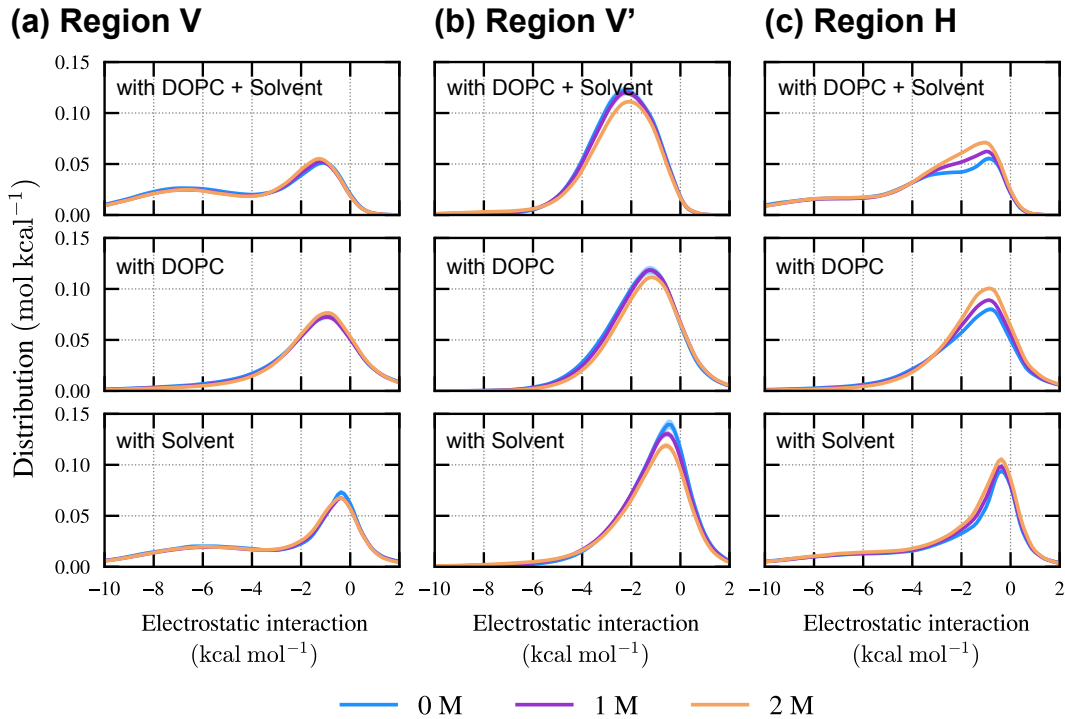


FIG. 5. Distributions of the electrostatic interaction energies between Prodan with its surrounding environments for (a) region V, (b) region V', and (c) region H. Top, middle, and bottom panels show the distributions of the interactions with DOPC and solvent (water and ethanol), with DOPC only, and with solvent only, respectively.

distort membrane structures.

The two-dimensional free-energy landscapes (2D-FELs) along the  $z$ -component of the center of mass (CoM) of Prodan and its orientation identified two stable regions within the membrane, in which the propionyl and dimethylamine groups of Prodan are respectively directed toward the aqueous phase. These regions were referred to as V and V', respectively, while the less stable region in which the molecular axis of Prodan is oriented perpendicular to the  $z$ -direction (normal to the membrane surface) was denoted as H. The stabilities of regions V and V' were similar, with V' being slightly more stable. The one-dimensional FELs (1D-FELs), restricted to a specific region, revealed that the orientational preferences in regions V and V' are mitigated by the addition of ethanol to the aqueous phase. The exact decomposition of the FELs into the interaction energy of Prodan with its surrounding environment and the many-body entropic contribution showed that the comparable stability of regions V and V' arises from a balance between stabilizing effects from the interaction energy contribution and destabilizing effects from the entropic contribution. The instability of region H, compared with the composite region of regions V and V', V + V', originated from the interaction energy near the membrane center and from the entropic contribution around  $z \sim 8$  Å. The stability difference between region H and V + V' decreased upon the addition of ethanol,

due to reduced differences in both the interaction-energy and the entropic contributions. Furthermore, the void-size distributions within the membrane suggest that the reduced destabilizing effects from the entropic contribution are correlated with a decrease in large voids near the membrane center. Such large voids can accommodate bulky molecules or moieties, so their reduction may lead to the relative destabilization of region V + V' when Prodan is located within  $z = 8 - 10$  Å, thereby reducing the stability difference. The electrostatic interaction of Prodan with its surrounding environment was stronger in the order  $V' > H > V$ , a trend primarily determined by its interaction with the solvent.

To further investigate a probe within membranes, incorporating a theoretical treatment of its electronic structure is an important step. Practically, the quantum mechanics/molecular mechanics (QM/MM) method is a useful approach for studying excitation properties in heterogeneous environments such as membranes. Osella *et al.*<sup>72</sup> and Wasif *et al.*<sup>31</sup> applied this method to investigate the excitation of probes within membranes, successfully characterizing their spectra. Recent advances in computing power and molecular dynamics (MD) software<sup>73</sup> have made it possible to combine QM/MM simulations with the REUS method for large-scale systems. Further elucidation using such a sophisticated technique would deepen our understanding of membrane properties through a more detailed interpretation of the spectra.

## ACKNOWLEDGMENTS

This work is supported by the Grants-in-Aid for Scientific Research (Nos. JP21H05249, JP23K27313, JP23K26617, JP25KJ1759, and JP25K17896) from the Japan Society for the Promotion of Science, the Fugaku Supercomputer Project (Nos. JPMXP1020230325 and JPMXP1020230327) and the Data-Driven Material Research Project (No. JPMXP1122714694) from the Ministry of Education, Culture, Sports, Science, and Technology, the Core Research for Evolutional Science and Technology (CREST) from Japan Science and Technology Agency (JST) (No. JPMJCR22E3), and by Maruho Collaborative Project for Theoretical Pharmaceuticals. The simulations were conducted using Genkai A at Kyushu University, and Fugaku at RIKEN Center for Computational Science through the HPCI System Research Project (Project IDs: hp250115, hp250211, hp250227, and hp250229).

## Appendix A: Definition of void-size distribution $P_V(z, \sigma)$

To analyze the distribution of voids within the membrane, defined as regions not occupied by atoms in the system, we employ a numerical technique for estimating void size, developed in the field of mesoporous material science.<sup>71</sup> The voids referred to here are called “pores” in that field. However, since “voids” is the term used in a recent membrane simulation study,<sup>70</sup> we adopt it in this work.

Let  $d_{V,\lambda}(z)$  denote the size of the  $\lambda$ th void whose center,  $\mathbf{x}_\lambda$ , lies between  $z$  and  $z + \Delta z$ . We suppose that all the voids located within this interval satisfy the following conditions.

$$\forall \lambda \leq N_V(z) \quad d_{V,\lambda}(z) = 2 \min_i \left( |\mathbf{x}_\lambda - \mathbf{r}_i| - \frac{\sigma_i}{2} \right), \quad (\text{A1})$$

$$\forall \lambda, \mu \leq N_V(z), \lambda \neq \mu \quad |\mathbf{x}_\lambda - \mathbf{x}_\mu| > \frac{1}{2} d_{V,\mu}(z). \quad (\text{A2})$$

$$\forall \lambda \leq N_V(z), \forall i \leq N_{\text{atom}} \quad |\mathbf{x}_\lambda - \mathbf{r}_i| > \frac{\sigma_i}{2}. \quad (\text{A3})$$

Here,  $\mathbf{r}_i$  is the position of  $i$ th atom in the system, and  $\sigma_i$  is its diameter.  $N_V(z)$  is the number of voids whose centers are located between  $z$  and  $z + \Delta z$ , and  $N_{\text{atom}}$  is the number of atoms in the system.  $d_{V,\lambda}(z)$  represents the maximum diameter of the sphere centered at  $\mathbf{x}_\lambda$  that does not contain any atoms. Eqs. (A2) and (A3) ensure that no void contains the center of any other void, and that all void centers are located outside the atoms in the system, respectively. Then, let us define the unnormalized void density as

$$\rho_V(z, \sigma) = \left\langle \frac{1}{\Delta z} \sum_{i=1}^{N_V(z)} \delta(\sigma - d_{V,i}(z)) \right\rangle. \quad (\text{A4})$$

Normalization is introduced as

$$P_V(z, \sigma) = \rho_V(z, \sigma) \left( \int_0^{z_P} dz \int_0^\infty d\sigma \rho_V(z, \sigma) \right)^{-1}. \quad (\text{A5})$$

Here,  $z_P$  is the average  $z$ -coordinate of the phosphorus atoms in DOPC molecules, measured from the membrane center ( $z = 0$ ).

The code for computing  $P_V(z)$  is implemented in PoreBlazer v4.0.<sup>71</sup> We use  $\sigma$  parameters of the Lennard-Jones interaction in the Universal force field (UFF)<sup>74</sup> as the atomic diameters,  $\sigma_i$ , in Eq. (A1).

## DATA AVAILABILITY

The data that support the findings of this study are available from the corresponding authors upon reasonable request.

- <sup>1</sup>P. L. Yeagle, *The structure of biological membranes* (CRC press, 2004).
- <sup>2</sup>Y. Komizu, S. Nakata, K. Goto, Y. Matsumoto, and R. Ueoka, *ACS Med. Chem. Lett.* **2**, 275 (2011).
- <sup>3</sup>X. Liu, B. Testa, and A. Fahr, *Pharm. Res.* **28**, 962 (2011).
- <sup>4</sup>D. B. Goldstein, *Annu. Rev. Pharmacol. Toxicol.* **24**, 43 (1984).
- <sup>5</sup>R. R. López, P. G. F. de Rubinat, L.-M. Sánchez, T. Tsering, A. Alazzam, K.-F. Bergeron, C. Mounier, J. V. Burnier, I. Stiharu, and V. Nerguizian, *Colloids Surf. B Biointerfaces* **198**, 111447 (2021).
- <sup>6</sup>L. K. Pershing, L. D. Lambert, and K. Knutson, *Pharm. Res.* **7**, 170 (1990).
- <sup>7</sup>R. Rai, D. Kumar, A. A. Dhule, B. A. Rudani, and S. Tiwari, *Langmuir* **40**, 14057 (2024).
- <sup>8</sup>J. R. Lakowicz, *Principles of fluorescence spectroscopy* (Springer, 2006).
- <sup>9</sup>G. Gunther, L. Malacrida, D. M. Jameson, E. Gratton, and S. A. Sánchez, *Acc. Chem. Res.* **54**, 976 (2021).
- <sup>10</sup>E. K. Krasnowska, E. Gratton, and T. Parasassi, *Biophys. J.* **74**, 1984 (1998).
- <sup>11</sup>P. Jurkiewicz, A. Olżyńska, M. Langner, and M. Hof, *Langmuir* **22**, 8741 (2006).
- <sup>12</sup>G. Weber and F. J. Farris, *Biochemistry* **18**, 3075 (1979).
- <sup>13</sup>R. B. Macgregor and G. Weber, *Nature* **319**, 70 (1986).
- <sup>14</sup>J. B. Massey and H. J. Pownall, *Biophys. J.* **74**, 869 (1998).
- <sup>15</sup>E. K. Krasnowska, L. A. Bagatolli, E. Gratton, and T. Parasassi, *Biochim. Biophys. Acta - Biomembr.* **1511**, 330 (2001).
- <sup>16</sup>T. Parasassi, G. De Stasio, G. Ravagnan, R. Rusch, and E. Gratton, *Biophys. J.* **60**, 179 (1991).
- <sup>17</sup>T. Parasassi, A. M. Giusti, M. Raimondi, and E. Gratton, *Biophys. J.* **68**, 1895 (1995).
- <sup>18</sup>T. Parasassi and E. Gratton, *J. Fluoresc.* **5**, 59 (1995).
- <sup>19</sup>T. Parasassi, E. K. Krasnowska, L. Bagatolli, and E. Gratton, *J. Fluoresc.* **8**, 365 (1998).
- <sup>20</sup>N. Ito, N. M. Watanabe, Y. Okamoto, and H. Umakoshi, *Biophys. J.* **122**, 4614 (2023).
- <sup>21</sup>N. Ito, N. M. Watanabe, Y. Okamoto, and H. Umakoshi, *Biophys. J.* **123**, 4135 (2024).
- <sup>22</sup>M. P. Allen and D. J. Tildesley, *Computer simulation of liquids* (Oxford university press, 1989).
- <sup>23</sup>D. Frenkel and B. Smit, *Understanding molecular simulation: from algorithms to applications*, Vol. 1 (Elsevier, 2001).
- <sup>24</sup>P. Jurkiewicz, L. Cwiklik, P. Jungwirth, and M. Hof, *Biochimie* **94**, 26 (2012).
- <sup>25</sup>S. Moradi, A. Nowroozi, and M. Shahlaei, *RSC Adv.* **9**, 4644 (2019).

- <sup>26</sup>L. Cwiklik, A. J. Aquino, M. Vazdar, P. Jurkiewicz, J. Pittner, M. Hof, and H. Lischka, *J. Phys. Chem. A* **115**, 11428 (2011).
- <sup>27</sup>W. K. Nitschke, C. C. Vequi-Suplicy, K. Coutinho, and H. Stassen, *J. Phys. Chem. B* **116**, 2713 (2012).
- <sup>28</sup>A. Suhaj, A. Le Marois, D. J. Williamson, K. Suhling, C. D. Lorenz, and D. M. Owen, *Phys. Chem. Chem. Phys.* **20**, 16060 (2018).
- <sup>29</sup>A. Suhaj, D. Gowland, N. Bonini, D. M. Owen, and C. D. Lorenz, *J. Phys. Chem. B* (2020).
- <sup>30</sup>S. Osella, N. A. Murugan, N. K. Jena, and S. Knippenberg, *J. Chem. Theory Comput.* **12**, 6169 (2016).
- <sup>31</sup>M. Wasif Baig, M. Pederzoli, P. Jurkiewicz, L. Cwiklik, and J. Pittner, *Molecules* **23**, 1707 (2018).
- <sup>32</sup>S. Osella and S. Knippenberg, *Biochim. Biophys. Acta - Biomembr.* **1863**, 183494 (2021).
- <sup>33</sup>S. Knippenberg, K. De, C. Aisenbrey, B. Bechinger, and S. Osella, *Cells* **13**, 1232 (2024).
- <sup>34</sup>Y. Sugita and Y. Okamoto, *Chem. Phys. Lett.* **314**, 141 (1999).
- <sup>35</sup>Y. Sugita, A. Kitao, and Y. Okamoto, *J. Chem. Phys.* **113**, 6042 (2000).
- <sup>36</sup>K. Murata, Y. Sugita, and Y. Okamoto, *Chem. Phys. Lett.* **385**, 1 (2004).
- <sup>37</sup>R. M. Venable, A. Krämer, and R. W. Pastor, *Chem. Rev.* **119**, 5954 (2019).
- <sup>38</sup>D. Bemporad, J. W. Essex, and C. Luttmann, *J. Phys. Chem. B* **108**, 4875 (2004).
- <sup>39</sup>Z. Ghaemi, M. Minozzi, P. Carloni, and A. Laio, *J. Phys. Chem. B* **116**, 8714 (2012).
- <sup>40</sup>C. T. Lee, J. Comer, C. Herndon, N. Leung, A. Pavlova, R. V. Swift, C. Tung, C. N. Rowley, R. E. Amaro, C. Chipot, *et al.*, *J. Chem. Inf. Model.* **56**, 721 (2016).
- <sup>41</sup>F. Cipcigan, P. Smith, J. Crain, A. Hogner, L. De Maria, A. Llinas, and E. Ratkova, *J. Chem. Inf. Model.* **61**, 263 (2020).
- <sup>42</sup>M. Sugita, S. Sugiyama, T. Fujie, Y. Yoshikawa, K. Yanagisawa, M. Ohue, and Y. Akiyama, *J. Chem. Inf. Model.* **61**, 3681 (2021).
- <sup>43</sup>Y. Matsubara, R. Okabe, R. Masayama, N. M. Watanabe, H. Umakoshi, K. Kasahara, and N. Matubayasi, *arXiv preprint arXiv:2404.11363* (2024).
- <sup>44</sup>A. A. Gurtovenko and J. Anwar, *J. Phys. Chem. B* **113**, 1983 (2009).
- <sup>45</sup>J. A. Barry and K. Gawrisch, *Biochemistry* **34**, 8852 (1995).
- <sup>46</sup>H. Rottenberg, *Biochemistry* **31**, 9473 (1992).
- <sup>47</sup>J. Zeng and P. Chong, *Biophys. J.* **68**, 567 (1995).
- <sup>48</sup>M. R. Shirts and J. D. Chodera, *J. Chem. Phys.* **129** (2008).
- <sup>49</sup>J. B. Klauda, R. M. Venable, J. A. Freites, J. W. O'Connor, D. J. Tobias, C. Mondragon-Ramirez, I. Vorobyov, A. D. MacKerell Jr, and R. W. Pastor, *J. Phys. Chem. B* **114**, 7830 (2010).
- <sup>50</sup>K. Vanommeslaeghe, E. Hatcher, C. Acharya, S. Kundu, S. Zhong, J. Shim, E. Darian, O. Guvench, P. Lopes, I. Vorobyov, *et al.*, *J. Comput. Chem.* **31**, 671 (2010).
- <sup>51</sup>W. L. Jorgensen, J. Chandrasekhar, J. D. Madura, R. W. Impey, and M. L. Klein, *J. Chem. Phys.* **79**, 926 (1983).
- <sup>52</sup>T. Yanai, D. P. Tew, and N. C. Handy, *Chem. Phys. Lett.* **393**, 51 (2004).
- <sup>53</sup>T. H. Dunning Jr, *J. Chem. Phys.* **90**, 1007 (1989).
- <sup>54</sup>C. M. Breneman and K. B. Wiberg, *J. Comput. Chem.* **11**, 361 (1990).
- <sup>55</sup>M. Frisch, G. Trucks, H. Schlegel, G. Scuseria, M. Robb, J. Cheeseman, G. Scalmani, V. Barone, G. Petersson, H. Nakatsuji, *et al.*, "Gaussian 16," (2016).
- <sup>56</sup>S. Jo, T. Kim, V. G. Iyer, and W. Im, *J. Comput. Chem.* **29**, 1859 (2008).
- <sup>57</sup>E. L. Wu, X. Cheng, S. Jo, H. Rui, K. C. Song, E. M. Dávila-Contreras, Y. Qi, J. Lee, V. Monje-Galvan, R. M. Venable, J. B. Klauda, and W. Im, *J. Comput. Chem.* **35**, 1997 (2014).
- <sup>58</sup>J. Lee, D. S. Patel, J. Stähle, S.-J. Park, N. R. Kern, S. Kim, J. Lee, X. Cheng, M. A. Valvano, O. Holst, *et al.*, *J. Chem. Theory Comput.* **15**, 775 (2018).
- <sup>59</sup>L. Martínez, R. Andrade, E. G. Birgin, and J. M. Martínez, *J. Comput. Chem.* **30**, 2157 (2009).
- <sup>60</sup>J. Jung, T. Mori, C. Kobayashi, Y. Matsunaga, T. Yoda, M. Feig, and Y. Sugita, *Wiley Interdiscip. Rev. Comput. Mol. Sci.* **5**, 310 (2015).
- <sup>61</sup>C. Kobayashi, J. Jung, Y. Matsunaga, T. Mori, T. Ando, K. Tamura, M. Kamiya, and Y. Sugita, *J. Comput. Chem.* **38**, 2193 (2017).
- <sup>62</sup>J. Jung, C. Kobayashi, K. Kasahara, C. Tan, A. Kuroda, K. Minami, S. Ishiduki, T. Nishiki, H. Inoue, Y. Ishikawa, *et al.*, *J. Comput. Chem.* **42**, 231 (2021).
- <sup>63</sup>G. Bussi, D. Donadio, and M. Parrinello, *J. Chem. Phys.* **126**, 014101 (2007).
- <sup>64</sup>W. C. Swope, H. C. Andersen, P. H. Berens, and K. R. Wilson, *J. Chem. Phys.* **76**, 637 (1982).
- <sup>65</sup>M. Bonomi and C. Camilloni, *Methods in Molecular Biology* **2022** (2019).
- <sup>66</sup>Y. Matsunaga, M. Kamiya, H. Oshima, J. Jung, S. Ito, and Y. Sugita, *Biophys. Rev.* , 1 (2022).
- <sup>67</sup>S. Sakuraba and N. Matubayasi, *J. Comput. Chem.* **35**, 1592 (2014).
- <sup>68</sup>W. Shinoda, M. Mikami, T. Baba, and M. Hato, *J. Phys. Chem. B* **108**, 9346 (2004).
- <sup>69</sup>A. E. Cardenas and R. Elber, *J. Chem. Phys.* **141**, 054101 (2014).
- <sup>70</sup>C. Chipot and J. Comer, *Sci. Rep.* **6**, 1 (2016).
- <sup>71</sup>L. Sarkisov, R. Bueno-Perez, M. Sutharson, and D. Fairen-Jimenez, *Chem Mater.* **32**, 9849 (2020).
- <sup>72</sup>S. Osella, N. A. Murugan, N. K. Jena, and S. Knippenberg, *J. Chem. Theory Comput.* **12**, 6169 (2016).
- <sup>73</sup>K. Yagi, K. Gunst, T. Shiozaki, and Y. Sugita, *J. Chem. Theory Comput.* (2025).
- <sup>74</sup>A. K. Rappé, C. J. Casewit, K. Colwell, W. A. Goddard III, and W. M. Skiff, *J. Am. Chem. Soc.* **114**, 10024 (1992).



# Supplement for “Characterizing the dissolution states of a fluorescent probe within a lipid bilayer using molecular dynamics simulations”

TABLE S1. Initial parameters for the restraint potentials for the REUS simulation ( $V_i(z) = k_i(z - z_i)^2$ ) in the case of the pure water phase. Subscript  $i$  represent the replica index.

Replica index	1	2	3	4	5	6	7	8
$k_i$ (kcal mol <sup>-1</sup> Å <sup>-2</sup> )	1.0	1.0	1.0	1.0	1.0	1.0	1.0	1.0
$z_i$ (Å)	0.00	1.00	2.00	3.00	4.00	5.00	6.00	7.00
Replica index	9	10	11	12	13	14	15	16
$k_i$ (kcal mol <sup>-1</sup> Å <sup>-2</sup> )	1.0	1.0	1.0	1.0	1.0	1.0	1.0	1.0
$z_i$ (Å)	8.00	9.00	10.00	11.00	12.00	13.00	14.00	15.00
Replica index	17	18	19	20	21	22	23	24
$k_i$ (kcal mol <sup>-1</sup> Å <sup>-2</sup> )	1.0	1.0	1.0	1.0	1.0	1.0	1.0	1.0
$z_i$ (Å)	16.00	17.00	18.00	19.00	20.00	21.00	22.00	23.00
Replica index	25	26	27	28	29	30	31	32
$k_i$ (kcal mol <sup>-1</sup> Å <sup>-2</sup> )	1.0	1.0	2.5	2.5	2.5	2.5	2.5	2.5
$z_i$ (Å)	24.00	25.00	25.60	26.20	26.80	27.40	28.00	28.60

TABLE S2. Optimized parameters for the restraint potentials used in the REUS simulation ( $V_i(z) = k_i(z - z_i)^2$ ) for the pure water phase. The initial parameters are listed in Table S1. Subscript  $i$  represent the replica index.

Replica index	1	2	3	4	5	6	7	8
$k_i$ (kcal mol <sup>-1</sup> Å <sup>-2</sup> )	1.0	1.0	1.0	1.0	1.0	1.0	1.0	1.0
$z_i$ (Å)	0.00	0.89	1.78	2.68	3.47	4.35	5.22	6.20
Replica index	9	10	11	12	13	14	15	16
$k_i$ (kcal mol <sup>-1</sup> Å <sup>-2</sup> )	1.0	1.0	1.0	1.0	1.0	1.0	1.0	1.0
$z_i$ (Å)	7.22	8.09	8.97	9.87	10.79	11.68	12.59	13.51
Replica index	17	18	19	20	21	22	23	24
$k_i$ (kcal mol <sup>-1</sup> Å <sup>-2</sup> )	1.0	1.0	1.0	1.0	1.0	1.0	1.0	1.0
$z_i$ (Å)	14.43	15.36	16.25	17.09	18.12	18.98	19.82	20.76
Replica index	25	26	27	28	29	30	31	32
$k_i$ (kcal mol <sup>-1</sup> Å <sup>-2</sup> )	1.0	1.0	2.5	2.5	2.5	2.5	2.5	2.5
$z_i$ (Å)	21.65	22.55	23.14	23.74	24.30	24.85	25.50	26.09

TABLE S3. Optimized parameters for the restraint potentials used in the REUS simulation ( $V_i(z) = k_i(z - z_i)^2$ ) for the 1 M ethanol aqueous phase. The initial parameters are taken from the optimized ones for the pure water case (Table S2). Subscript  $i$  represent the replica index.

Replica index	1	2	3	4	5	6	7	8
$k_p$ (kcal mol <sup>-1</sup> Å <sup>-2</sup> )	1.0	1.0	1.0	1.0	1.0	1.0	1.0	1.0
$z_i$ (Å)	0.00	0.87	1.76	2.63	3.52	4.50	5.39	6.32
Replica index	9	10	11	12	13	14	15	16
$k_i$ (kcal mol <sup>-1</sup> Å <sup>-2</sup> )	1.0	1.0	1.0	1.0	1.0	1.0	1.0	1.0
$z_i$ (Å)	7.17	8.13	9.07	9.98	10.93	11.79	12.53	13.38
Replica index	17	18	19	20	21	22	23	24
$k_i$ (kcal mol <sup>-1</sup> Å <sup>-2</sup> )	1.0	1.0	1.0	1.0	1.0	1.0	1.0	1.0
$z_i$ (Å)	14.22	15.13	16.05	16.93	17.69	18.63	19.63	20.62
Replica index	25	26	27	28	29	30	31	32
$k_i$ (kcal mol <sup>-1</sup> Å <sup>-2</sup> )	1.0	1.0	2.5	2.5	2.5	2.5	2.5	2.5
$z_i$ (Å)	21.38	22.27	22.79	23.34	23.90	24.51	25.11	25.66

TABLE S4. Optimized parameters for the restraint potentials used in the REUS simulation ( $V_i(z) = k_i(z - z_i)^2$ ) for the 2 M ethanol aqueous phase. The initial parameters are taken from the optimized ones for the pure water case (Table S2). Subscript  $i$  represent the replica index.

Replica index	1	2	3	4	5	6	7	8
$k_p$ (kcal mol <sup>-1</sup> Å <sup>-2</sup> )	1.0	1.0	1.0	1.0	1.0	1.0	1.0	1.0
$z_i$ (Å)	0.00	0.85	1.61	2.57	3.44	4.37	5.21	6.16
Replica index	9	10	11	12	13	14	15	16
$k_i$ (kcal mol <sup>-1</sup> Å <sup>-2</sup> )	1.0	1.0	1.0	1.0	1.0	1.0	1.0	1.0
$z_i$ (Å)	7.04	8.00	8.86	9.68	10.50	11.47	12.48	13.31
Replica index	17	18	19	20	21	22	23	24
$k_i$ (kcal mol <sup>-1</sup> Å <sup>-2</sup> )	1.0	1.0	1.0	1.0	1.0	1.0	1.0	1.0
$z_i$ (Å)	14.25	15.07	16.13	17.05	17.94	18.88	19.87	20.80
Replica index	25	26	27	28	29	30	31	32
$k_i$ (kcal mol <sup>-1</sup> Å <sup>-2</sup> )	1.0	1.0	2.5	2.5	2.5	2.5	2.5	2.5
$z_i$ (Å)	21.69	22.58	23.16	23.82	24.35	25.00	25.67	26.23

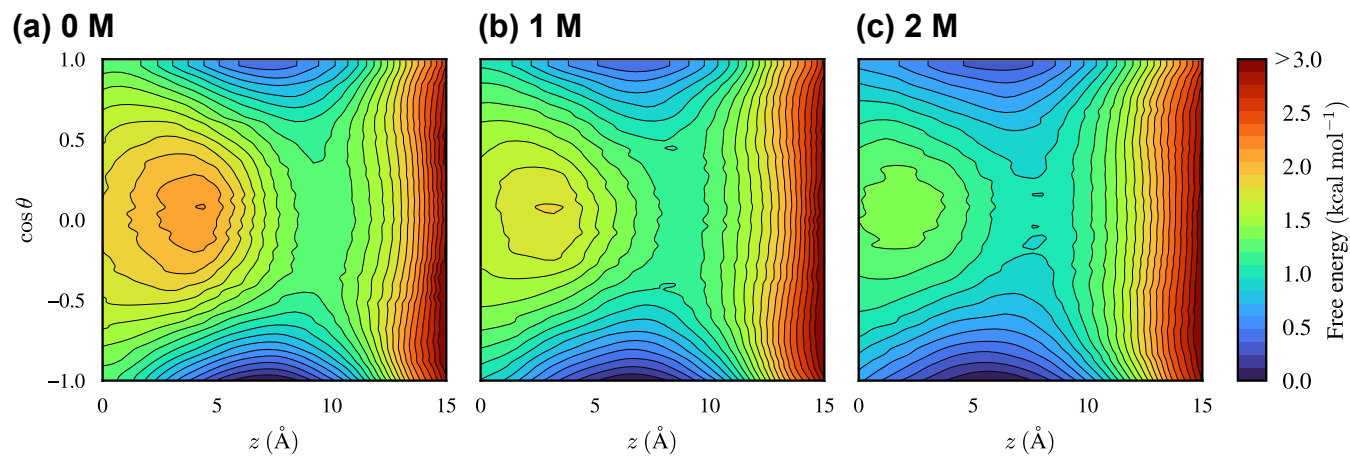


FIG. S1. Free-energy landscapes on the  $z$ -component of the center of mass (CoM) for Prodan,  $z$ , and the cosine of the title angle,  $\cos \theta$ , for (a) pure water, (b) 1 M ethanol, and (c) 2 M ethanol aqueous phases.

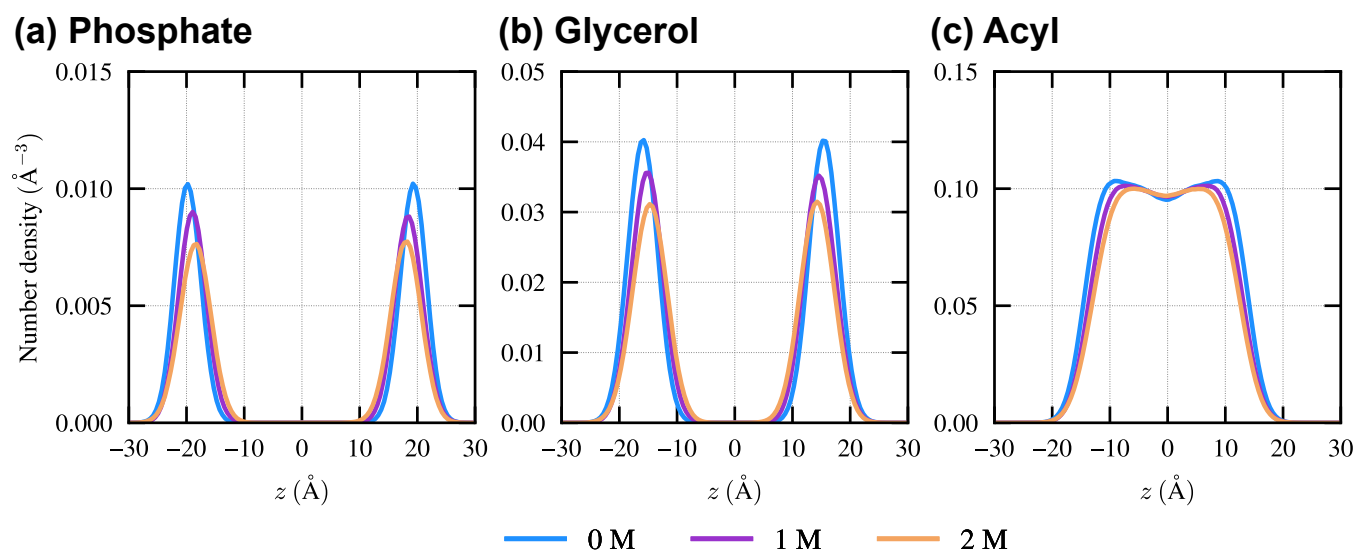


FIG. S2. Distributions along the  $z$ -direction of atoms in (a) phosphate group, (b) glycerol group, and (c) acyl chains.